High-Power Nanostructured $LiMn_{2-x}Ni_xO_4$ High-Voltage Lithium-Ion Battery Electrode Materials: Electrochemical Impact of Electronic Conductivity and Morphology

Muharrem Kunduraci,*[,†,‡] Jafar F. Al-Sharab,[‡] and Glenn G. Amatucci[†,‡]

Energy Storage Research Group, Department of Materials Science and Engineering, Rutgers, The State University of New Jersey, North Brunswick, New Jersey 08902

Received March 27, 2006. Revised Manuscript Received May 10, 2006

The direct relationship between the electronic conductivity of the nanostructured spinel $LiMn_{2-x}Ni_xO_4$ and its lattice parameter is reported. Within the 8.167−8.183 Å range studied, there was a systematic 2.5 orders of magnitude difference between the highest electronic conductivity (cation disordered *Fd*3*m* spinel) to lowest conductivity (ordered $P4_332$ spinel). The underlying reason behind the higher conductivity of the former was the presence of Mn^{3+} (nonexistent in ordered) and Mn^{4+} sites. The impact of the observed electronic conductivity on electrochemical performance is discussed with respect to morphological impact on ion diffusion and power delivery in various electrode formulations.

Introduction

The growing interest to employ lithium-ion batteries for high-power applications, e.g., hybrid electric vehicle, has induced an extensive research effort worldwide. Critical to the realization of high-power delivery is to design a cathode material offering high-energy density at fast discharge rates. This necessitates the electroactive material to have both high electronic and ionic conductivities. The literature contains many examples dedicated to the enhancement of the rate capability of the cathode by increasing its nonintrinsic electronic conductivity by coating with a conductive agent.[1−5] With regard to ionic conduction, selection of nanosize particles has resulted in high lithium-ion transport since bulk diffusion length is significantly reduced in nanostructured samples.[6−7] Another way of increasing the power density of battery comes from the utilization of high-voltage cathodes that offer an increase in energy density without necessitating an increase in the current density of the nonaqueous electrolyte system, which is already limited by poor conductivity. The transition-metal-doped spinel-type $LiMn_{2-x}M_xO_4$ (where M is Ni,[8,9] Fe,[10,11] Cr,[12] Co[13,14] etc.) offers one of the highest potentials yet known. The mechanism is based on oxidation/reduction of the doped transition metal above 4.6 V. Among all possible compositions $LiMn_{1.5}Ni_{0.5}O_4$ is the most attractive since it offers a flat plateau at 4.7 V, has a capacity >130 mA·h/g, and has been demonstrated to show good cycling stability and rate capability.

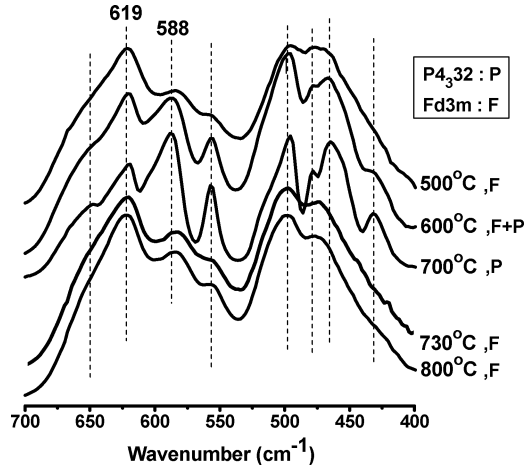

Figure 1. Infrared spectra of ordered ($P4_332$) and disordered (*Fd*3*m*) $LiMn_{1.5}Ni_{0.5}O_4$ as a function of synthesis temperature. The intensity ratio of two bands at 619 and 588 cm^{-1} can be used qualitatively to assess percentage of ordering in spinel.

In an earlier work[15] we showed via infrared spectroscopy (Figure 1) that $LiMn_{1.5}Ni_{0.5}O_4$ spinel undergoes a thermally induced order → disorder transition between 700 and 730 °C. In ordered $P4_332$ phase, Mn^{4+} and Ni^{2+} ions are ordered

* Corresponding author. E-mail: muharrem@eden.rutgers.edu. Phone: 732-932-6850 (608). Fax: 732-932-6855.
† Energy Storage Research Group.
‡ Department of Materials Science.

(1) Shizuka, K.; Kobayashi, T.; Okahara, K.; Okamoto, K.; Kanzaki, S.; Kanno, R. *J. Power Sources* **2005**, *146*, 589.
(2) Xie, H.; Zhou, Z. *Electrochim. Acta* **2006**, *51*, 2063.
(3) Huang, S.; Wen, Z.; Yang, X.; Gu, Z.; Xu, X. *J. Power Sources* **2005**, *148*, 72.
(4) Park, S.-H.; Kim, Y.-M.; Kang, Y.-M.; Kim, K.-T.; Lee, P.-S.; Lee, J.-Y. *J. Power Sources* **2001**, *103*, 86.
(5) Chung, S.-Y.; Bloking, J.-T.; Chiang, Y.-M. *Nature* **2003**, *1*, 123.
(6) Prosini, P.-P.; Carewska, M.; Scaccia, S.; Wisniewski, P.; Pasquali, M. *Electrochim. Acta* **2003**, *48*, 4205.
(7) Franger, S.; Benoit, C.; Bourbon, C.; Cras, F.-L. *J. Phys. Chem. Solids* **2006**.
(8) Zhong, Q.; Bonakdarpour, A.; Zhang, M.; Gao, Y.; Dahn, J.-R. *J. Electrochem. Soc.* **1997**, *144*, 205.
(9) Lazarraga, M.-G.; Pascual, L.; Gadjov, H.; Kovacheva, D.; Petrov, K.; Amarilla, J.-M.; Rojas, R.-M.; Martin-Luengo, M.-A.; Rojo, J.-M. *J. Mater. Chem.* **2004**, *14*, 1640.
(10) Eftekhari, A. *J. Power Sources* **2003**, *124*, 182.
(11) Ohzuku, T.; Ariyoshi, K.; Takeda, S.; Sakai, Y. *Electrochim. Acta* **2001**, *46*, 2327.
(12) Wang, H.-C.; Lu, C.-H. *J. Power Sources* **2003**, *119*−*121*, 738.
(13) Wu, S.-H.; Su, H.-J. *Mater. Chem. Phys.* **2002**, *78*, 189.
(14) Kawai, H.; Nagata, M.; Kageyama, H.; Tukamato, H.; West, A.-R. *Electrochim. Acta* **1999**, *45*, 315.
(15) Kunduraci, M.; Amatucci, G.-G. *J. Electrochem. Soc.* **2006**, *153* (7).

10.1021/cm060729s CCC: $33.50
Published on Web 07/01/2006

on octahedral sites in a 3:1 ratio as opposed to random distribution in disordered *Fd*3*m* phase. The coincidence of this temperature range with the onset temperature (712 °C) for oxygen loss in thermogravimetric analysis suggested that this transition is driven by oxygen deficiency in spinel, resulting in the manifestation of Mn^{3+} ions above this temperature to satisfy the charge balance in spinel structure. A $Li_yNi_{1-y}O$ phase was also observed as a secondary phase, consistent with an earlier report.[8] Understandably, the oxygen loss accelerates with more residence time spent at higher temperatures above the onset temperature, thereby causing larger Mn^{3+} concentration in disordered spinel and more secondary phase. Within the 500−800 °C range investigated, the lattice volume of spinel, which can be described to have a v-shape dependence on synthesis temperature, had its minimum value at 700 °C. The concurrence of this trend with phase transition temperature was supportive to the argument that phase transition is associated with partial substitution of smaller Mn^{4+} ions by larger Mn^{3+} ions, which was absent in ordered state.

After detailed electrochemical characterization, the cation disordered spinel was found to outperform the ordered spinel at fast discharge rates in accordance with an earlier study.[16] As opposed to the previous work in which the difference was based on an electrochemically induced order−disorder transition undergone by ordered spinel during lithiation, we attributed the poor rate capability of the latter to its lower electronic conductivity.

In producing nanosize powders, methods based on wet synthesis have many advantages relative to traditional techniques such as solid-state synthesis or mechanical milling. We have chosen a modified Pechini method due to its simplicity and high yield in quantity and quality of mesoporous, networked powders. Here, we report high discharge voltage cathodes with extreme rate capabilities due to optimization of the electronic conductivities and unique nanostructure. This paper was divided into two parts. In the first part, the correlation between electronic conductivity and lattice constant, Mn^{3+} content, and ordering of the $LiMn_{1.5}Ni_{0.5}O_4$ spinel was investigated. In the second, a similar correlation was investigated between electronic conductivity and discharge rate capability of $LiMn_{2-x}Ni_xO_4$ spinels to complete the observed connection between rate capability and ordering of 4.7 V spinels.

Experimental Section

Synthesis. The $LiMn_{2-x}Ni_xO_4$ powders were synthesized by a modified Pechini process.[17] A 1:4 molar ratio of citric acid−ethylene glycol solution was heated to 90 °C under constant stirring. Once the solution became clear, another solution consisting of required stoichiometric amounts of $Li(NO_3)$, $Mn(NO_3)_2 \cdot 4H_2O$, and $Ni(NO_3)_2 \cdot 6H_2O$, which were initially dissolved in a minimum amount of distilled water, was added dropwise to the former aqueous solution. A 1:1 mole ratio of metal ions to citric acid was chosen. The solution was kept at this temperature for an hour for the completion of the chelation process. After this point the process described in a earlier study[14] was modified such that instead of keeping the solution in a beaker at 140 °C until it turned into a glassy-like solid, the viscous solution was cast and spread on a 4 × 6 in. stainless steel plate that was preheated to 140 °C. After the batch was fully free from excess water and ethylene glycol, it was ignited in open air. The sample was ground and heated to an elevated temperature for annealing. The annealing temperature was selected as 500 °C for the precursor powders used in the electrical conductivity measurements in Part I and 700 °C for electrochemical study in Part II.

XRD, FTIR. X-ray powder diffraction (XRD) was taken using a Scintag X2 Inc. diffractometer. Each sample was scanned between 15° and 90° at a rate of 0.1°/min using Cu Kα radiation. A silicon standard was used for lattice constant measurements. A Thermonicolet Avatar 360 was used for a Fourier-transformed infrared (FTIR) study. The spectra of spinels were obtained by diluting a minute amount of powder in 100 mg of KBr powder. Each datum was an average of 100 scans taken between 4000 and 400 cm^{-1}.

FESEM, TEM, BET. The TEM samples were prepared by dispersing spinel powder in methanol and releasing a few drops of the liquid on an amorphous "lacey" carbon film supported on copper grid. The mixture then was allowed to dry, leaving behind particles dispersed on the TEM grid. The grids were sealed under helium. HRTEM images were obtained using a Topcon 002B microscope operating at 200 kV. The SEM samples were prepared by directly placing the bulk powder on a conducting carbon tape. GEMINI FESEM 982 was used to study the morphologies of powders. Micromeritics ASAP 2000 was used for BET surface area measurements.

For ac impedance spectroscopy measurements, the fresh powders were preheated to 500 °C for 10 h and cooled to room temperature. They were later compacted under 200 MPa pressure and subjected to various heat treatments. The same procedure was repeated for 15 samples so as to obtain lattice constants between 8.167 and 8.183 Å. The thickness of sintered pellets ranged from 0.8 to 2 mm. Careful attention was made to have pellets of similar densities of approximately 80−82%. The diameter of pellet disks was about 1.2 cm. Both surfaces of pellets were polished and painted with conductive silver paste to conduct electrical measurements. The pellets were embedded in a stainless steel swagelok cell. The cell was later covered with a polylaminate bag and immersed into a 2-propanol bath. Both ends of swagelok were connected to Solartron 1287 and 1260 impedance analyzer via copper wires. An ac frequency range from 0.01 Hz to 1 MHz was chosen. The ac conductivity measurements were performed between −25 and 40 °C. Each measurement was performed approximately 1 h after the temperature reached the set value. A 20 mV ac potential, which was increased to 100 mV for measurements at low temperatures, was applied on pellets. The *I*/*V* behavior was linear up to a few hundred millivolts.

Electrochemical Characterization. 2025 type coin cells were used for the electrochemical characterization of $LiMn_{2-x}Ni_xO_4$ powders. The cell consisted of $LiMn_{2-x}Ni_xO_4$ as the positive electrode, Li metal as the negative electrode, and 1 M $LiPF_6$ dissolved in a mixture of EC-DMC as the electrolyte. The positive electrode was fabricated by the Bellcore process composed of a mixture of various weight percentages of active material (65 − *x* wt %), Super P carbon black (MMM) (*x* wt %) poly(vinylidene fluoride-*co*-hexafluoropropylene) (PVDF−HFP) (Kynar 2801, Elf Atochem) binder (35 wt %) dispersed in dibutyl phthalate (DBP) (Aldrich) plasticizer. The slurry was cast and dried in air at room temperature. Afterward the DBP plasticizer was removed through successive extractions in ether. The dried electrodes were then

(16) Kim, J.-H.; Myung, S.-T.; Yoon, C.-S.; Kang, S.-G.; Sun, Y.-K. *Chem. Mater.* **2004**, *16*, 906.
(17) Liu, W.; Farrington, G.-C.; Chaput, F.; Dunn, B. *J. Electrochem. Soc.* **1996**, *143*, 879.

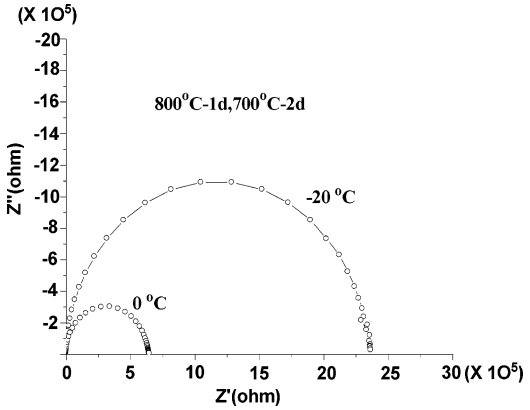

Figure 2. Nyquist plots at 0 and −20 °C of $LiMn_{1.5}Ni_{0.5}O_4$ pellet sintered at 800 °C for 1 day and postannealed at 700 °C for 2 days.

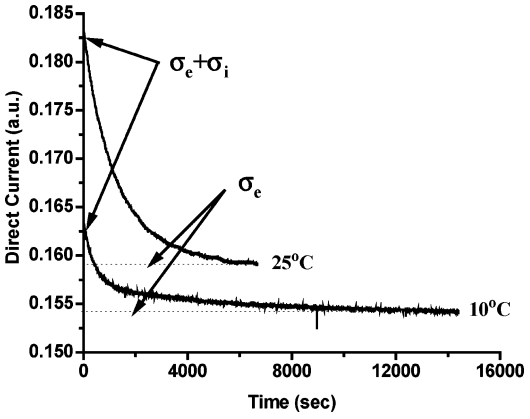

Figure 3. Direct current decay profile of two nonidentical pellets at 10 and 25 °C. The arrows show the contributions from electronic and ionic conduction.

further dried at 120 °C for 12 h under vacuum. The cell was assembled in a He-filled glovebox and cycled using a Maccor galvanostat cycler. The weight of active material was 2.4−2.6 mg/cm^2 for all samples in Part II. The cells were electrochemically cycled between 3.5 and 5 V.

Results and Discussion

I. Electrical Conductivity and Crystal Structure. The Nyquist plots of $LiMn_{1.5}Ni_{0.5}O_4$ pellet heat-treated at 800 °C for 1 day and postannealed at 700 °C for 2 days (hereafter, a pellet is named with its sintering temperature and time, e.g., 800 °C-1d, 700 °C-2d) and analyzed at 0 °C and −20 °C are given in Figure 2 as representatives of all samples. An *RC* unit was used for fitting. Due to the mixed conductor nature of spinels, dc polarization measurements were also performed at 0, 10, and 25 °C to calculate the percent contribution of ionic conduction to overall conductivity. In Figure 3, direct current decay profiles of two representative samples of identical composition are given for 10 and 25 °C. The percentage of current due to the ionic contribution was calculated to be approximately 1−2, 4−5, and 10−15% at 0, 10, and 25 °C, respectively. It was concluded that contribution of ionic conduction is negligible to the overall conduction below 10 °C and it was excluded in Arrhenius plots of pellets which were mostly performed in the low-temperature regime.

The Arrhenius plots of pellets are given in Figure 4. All samples show a linear dependence with inverse of temperature. The goodness-of-fit (R) was better than 0.9996 (for all 15). Only 7 out of 15 pellets are shown in order to simplify the plot and draw the attention to a particular behavior. This is presented in two ways; (i) transitioning from ordered 700 °C-2d spinel to disordered 730 °C-2d, the conductivity increased by 1.5 orders of magnitude (arrow 3); (ii) 850 °C-2d pellets were reannealed at four different temperatures, namely, 775, 730, 700, and 600 °C. For reannealing temperatures larger than the oxygen loss onset temperature (712 °C), the spinel retained its disordered structure and kept its high conductivity prior to reannealing. For reannealing temperatures below onset temperature, disordered spinel transformed to ordered phase and its conductivity decreased by 1−1.5 orders of magnitude (arrows 1 and 2). The conversion to ordered $P4_332$ was substantiated by infrared spectroscopy.

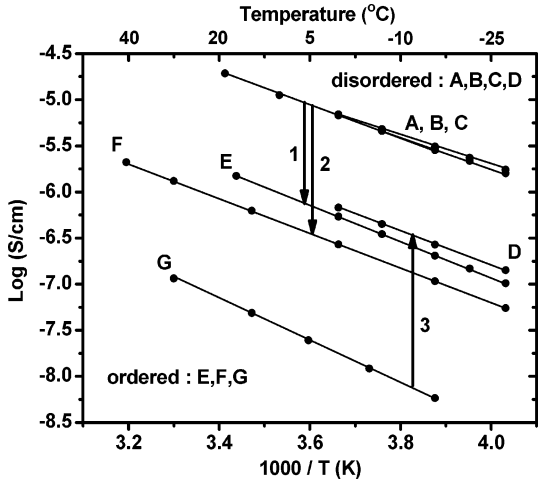

Figure 4. Arrhenius plots of $LiMn_{1.5}Ni_{0.5}O_4$ pellets. A: (850 °C-2d); B: (850 °C-2d, 775 °C-3d); C: (850 °C-2d, 730 °C-3d); D: (730 °C-2d); E: (850 °C-2d, 700 °C-3d); F: (850 °C-2d, 600 °C-3d); G: (700 °C-2d).

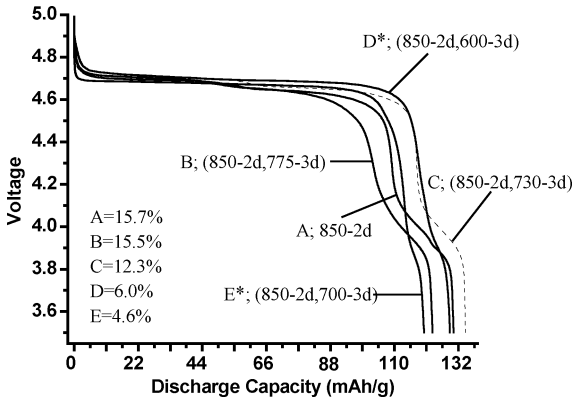

Figure 5. Galvanostatic discharge curves of $LiMn_{1.5}Ni_{0.5}O_4$ pellets. The numbers in percent represent the ratio of capacity in the 4 V region to overall capacity. It is zero for the (700 °C-2d) sample (not included).

To further define the characteristics of the pelletized samples used for conductivity studies, unpainted sister pellets of the seven pellets analyzed were ground and subjected to galvanostatic analysis, Figure 5. The percentage of discharge capacity in 4 V plateau (%4V), which corresponds to $Mn^{4+} + e^- \rightarrow Mn^{3+}$ transition, was characterized relative to overall capacity. In the case of the (850 °C-2d, 730 °C-3d) pellet the %4V is slightly smaller than those of (850 °C-2d, 775

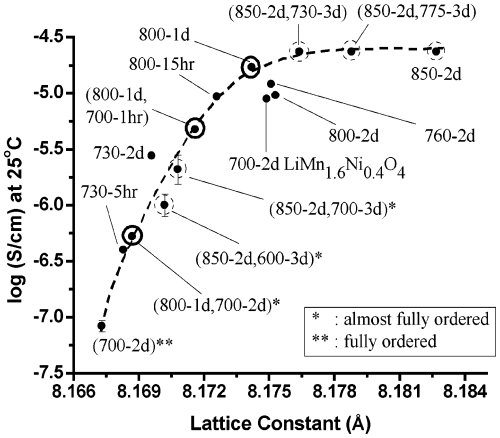

Figure 6. Room-temperature conductivities of $LiMn_{1.5}Ni_{0.5}O_4$ pellets with respect to their lattice constants. Pellets with similar thermal history are circled in the same way. The dotted line shows the trend to guide the eye.

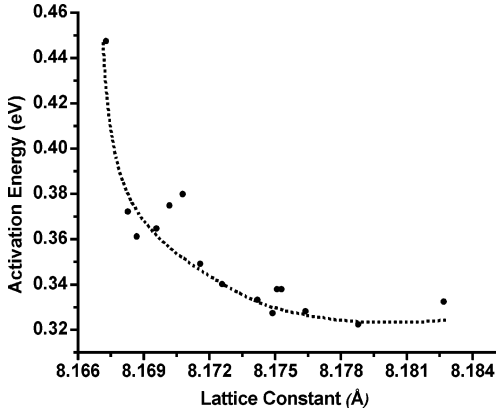

Figure 7. Dependence of activation energy of electron hopping on lattice constant of $LiMn_{1.5}Ni_{0.5}O_4$. The dotted line indicates the critical point, mentioned in the text.

°C-2d) and nonannealed pellet. This suggests, as expected, that after the reannealing at 730 °C the pellets restored a small degree of the oxygen they lost during initial heating to 850 °C. As for (850 °C-2d, 700 °C-3d) and (850 °C-2d, 600 °C-3d) samples, they have much smaller 4 V capacity, clearly showing that these samples were reoxidized to almost pure Mn^{4+}.

Plotting the room-temperature conductivities of all pellets with respect to their lattice constants resulted in the development of a distinct trend (Figure 6). A strong continuous increase of conductivity with lattice constant occurs until a critical point at 8.1765 Å is reached. After this point conductivity becomes independent of lattice constant within the lattice constant regime studied. The larger lattice constant region (disordered *Fd*3*m* spinel) is associated with an increase in Mn^{3+}/Mn^{4+} ratio and percentage of secondary $Li_yNi_{1-y}O$ phase. Hence, the enhancement of conductivity may be based on either of these factors. Knowing that electron hopping between Mn^{3+} and Mn^{4+} is the electronic conduction mechanism in the isostructural spinel $LiMn_2O_4$, it would not be wrong to predict that electron hopping rather than the secondary phase might be the basis of higher conductivity in disordered spinels. To ascertain the validity of this prediction, we synthesized $LiMn_{1.6}Ni_{0.4}O_4$ at 700 °C for 15 h and compared its conductivity with those of other spinels since, due to the Mn/Ni stoichiometry change, this spinel (i) is free from second phase, (ii) has a lattice constant within the range of interest, and (iii) has a significant Mn^{3+} population. In short, this composition is similar to the large lattice parameter samples with respect to high Mn^{3+} content but without the presence of a second phase. Since this phase has about 20% of its capacity at 4 V discharge potential, in theory its conductivity should be equal to that of the 850 °C-2d pellet if conductivity was solely dependent on the Mn^{3+} content and independent of second phase formation. As given in the same figure, $LiMn_{1.6}Ni_{0.4}O_4$ has a similar conductivity to the latter's, which rules out the $Li_yNi_{1-y}O$ phase to be the origin of the high conduction in the *Fd*3*m* samples. Another conclusion is that depending on the average manganese valency, the difference between ordered and disordered $LiMn_{1.5}Ni_{0.5}O_4$ can be as much as 2.5 orders of magnitude.

In many of the results presented above, there seems to be a gray area (see pellets marked with * in Figures 5 and 6) between fully ordered $P4_332$ material and disordered *Fd*3*m* material with high lattice constant. This area has been entered through postannealing of disordered spinels at 600 or 700 °C (the annealing time was long enough to enable disorder−order transformation). Characterization by infrared spectroscopy shows a continuous decreasing quantity of ordered character scaling with increasing Mn^{3+} content. An important point that needs to be addressed here is in regards to the nature of local area around Mn^{3+} cations, i.e., presence of cation ordering or disordering in the vicinity of these cations. The existence of 4 V plateau and ordering in these samples bring up two scenarios: (1) Ordered spinel can dissolve small amounts of Mn^{3+} (Mn^{3+} corresponds to about 4% of overall manganese ions in the case of (850 °C-2d, 700 °C-3d)) and these ions are distributed evenly throughout the ordered spinel. (2) No Mn^{3+} can reside in ordered spinel crystallite, causing cation disordered crystallites to form in the local area. This implies the coexistence of two structures next to each other at nanoscale in the same crystal. As the materials are very sensitive to oxygen content, such a phase segregation may exist radially within the primary particle. Selective area electron diffraction will be utilized in future work to discern these scenarios.

The activation energies of pellets are plotted in Figure 7. The energy barrier for conduction reaches its highest value at 0.45 eV in fully ordered spinel. With the introduction of small amounts of Mn^{3+}, this barrier is reduced 0.36 eV and can be systematically reduced to a minimum of 0.32 eV with further addition of this ion. The ease of conduction going from ordered state to disordered is in agreement with the previous figure and increase of Mn^{3+} quantity.

II. Electrochemical Measurements. As mentioned in the Introduction, we have shown in our previous work that cation ordered $P4_332$ spinel exhibits less capacity retention than disordered spinel at fast discharge rates. Sun et al.[16] suggested an electrochemically induced order−disorder transition in this space group be the basis for its poor electrochemical performance. However, we believe it has an electronic conductivity origin as the ordered structure has up to 2.5 orders of magnitude lower electronic conductivity, a must for good rate capability. If our claim were true, then

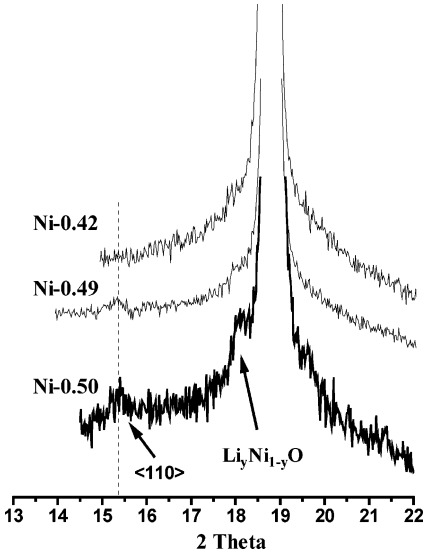

Figure 8. XRD spectra of Ni-*x* samples (*x* in LiMn$_{2-x}$Ni$_x$O$_4$). Dotted line indicates the position of superlattice ⟨110⟩ peak present in Ni-0.50 and Ni-0.49. A small secondary peak with Ni-0.50 is also seen, which can be ignored for the sake of discussion.

increasing percentage of Super P would indeed compensate for lower conductivity of ordered spinel and raise its performance to the same levels of the disordered one but have no impact on any intrinsic structural changes or Mn^{3+} content. In this respect, we have fabricated electrodes from LiMn$_{2-x}$Ni$_x$O$_4$ cathode active material with varying weight percentages of Super P. The composition of tapes was formulated as follows: 35 wt % PVDF−HFP binder, *x* wt % Super P, and (65 − *x*) wt % active material, where *x* = 4, 6.5, 10, or 13.

We chose to synthesize and study LiMn$_{2-x}$Ni$_x$O$_4$ for *x* = 0.50, 0.49, 0.42, or 0.40 (hereafter the spinel will be named as Ni-*x*). The X-ray diffraction spectra of synthesized samples in the range 13°−22° are given in Figure 8. Both Ni-0.50 and Ni-0.49 have ⟨110⟩ superlattice peak, confirming cation ordering in these structures. Infrared spectroscopy also affirmed ordering. Due to similarities in terms of structure and %4V (or %Mn^{3+}), Ni-0.49 and Ni-0.42 were intended to be similar in performance and characteristics of the Ni-0.50 and Ni-0.40 spinels, respectively.

The active material loading was intentionally kept low at 2.4−2.6 mg/cm^2 to minimize the side effects of cell polarization such that a true comparison of performances of ordered and disordered spinels without being undermined by outside factors could be performed. The discharge currents were selected as 0.7, 1.5, and 2.5 A/g, which are situated in a range sufficiently low (∼5 C) and high (19 C). The summary of electrochemical measurements is given in Table 1. The following conclusions have been made.

(1) The rate capability of both ordered ($P4_332$) and disordered ($Fd3m$) spinels increase with increasing wt % Super P up to 10%. Further increase of conduction agent does not contribute to the performance or even may cause a slight degradation. A possible reason is that electronic limitations for power capability end at this point, reaching a limit around 10−13 wt %.

(2) There is no significant difference between the ordered $P4_332$ and disordered $Fd3m$ spinels in cases of 10 and 13 wt % Super P. However, disordered spinels outperform ordered ones significantly in cases of 6.5 and 4 wt % of conductive agent. This, with little doubt, supports our claim that the source of the electrochemical performance difference between the two space group spinels has an electronic conductivity origin as the lower percentages of the Super P require the spinels to conduct more of the current through bulk/surface pathways.

(3) The discharge capacity and average discharge voltage output of samples increase with more use of Super P consistent with decreasing IR component.

(4) The 1st and 2nd cycle Coulombic efficiency is almost independent of amount of conductive agent. This suggests that the high surface area conductive black is not adding much to the irreversible loss experienced on the first cycle at high voltages.

(5) The two plateaus around 4.7 V were better resolved with higher wt % of Super P.

Since all four sample compositions were synthesized at 700 °C, which is below the onset temperature for oxygen loss, they all should be treated as oxygen stoichiometric, assuming that onset temperature lies above 700 °C irrespective of nickel content. To identify if oxygen loss or change in morphology of particles would have any impact on electrochemical performances of spinels, Ni-0.49 and Ni-0.40 samples (as representative of ordered $P4_332$ and disordered $Fd3m$, respectively) were heated to 730 °C. The samples were reannealed at this temperature for just 2 h to avoid excessive formation of Mn^{3+} (denoted as Ni-0.49*, which transformed from $P4_332$ to $Fd3m$, and Ni-0.40*, respectively). The results are reported in the same table. Both samples followed the same trends mentioned above. However, not only their rate capabilities were higher in magnitude

Table 1. Summary of Electrochemical Performances of Ni-*x* (*x* in LiMn$_{2-x}$Ni$_x$O$_4$) Given with Their Specific Surface Area[a]

sample	space group	% capacity (at 0.7-1.5-2. 5 A/g) when wt % SP = 4%	6.5%	10%	13%	BET surface area (in m^2/g)	discharge capacity with 4%/13% SP
Ni-0.50	$P4_332$	51-27-6	72-54-40	88-78.5-68.7	88.5-77.6-68	7.98 ± 0.12	115/129
Ni-0.49	$P4_332$	46-30-17	65-47-35	84-72-62	NA	8.57 ± 0.13	104/−
Ni-0.42	$Fd3m$	72-45-25	85-70-57	89-77-66.6	NA	8.18 ± 0.16	118/−
Ni-0.40	$Fd3m$	66-41-19	89-70-53	92-80.5-67	91-78-62	6.17 ± 0.16	128/142
Ni-0.49*	$Fd3m$	77-54-19	87-77-65	95-88-80	93-87-81.6	8.58 ± 0.06	130/142
Ni-0.40*	$Fd3m$	NA	NA	NA	95-86-75	5.42 ± 0.14	−/133.5
Ni-0.49**	$Fd3m$	NA	NA	NA	95-92-87	7.27 ± 0.07	−/132
Ni-0.50**	$Fd3m$	NA	NA	NA	93-89-83	NA	−/132

[a] The percent relative capacities are with respect to those when discharged at 22 mA/g. Discharge capacities are given in mA·h/g. The heat treatments are (700 °C-15h, 730 °C-2h) for samples marked with *, (730 °C-1h) for those with **, and (700 °C-15h) otherwise. Only Ni-0.50 and Ni-0.49 are cation ordered $P4_332$.

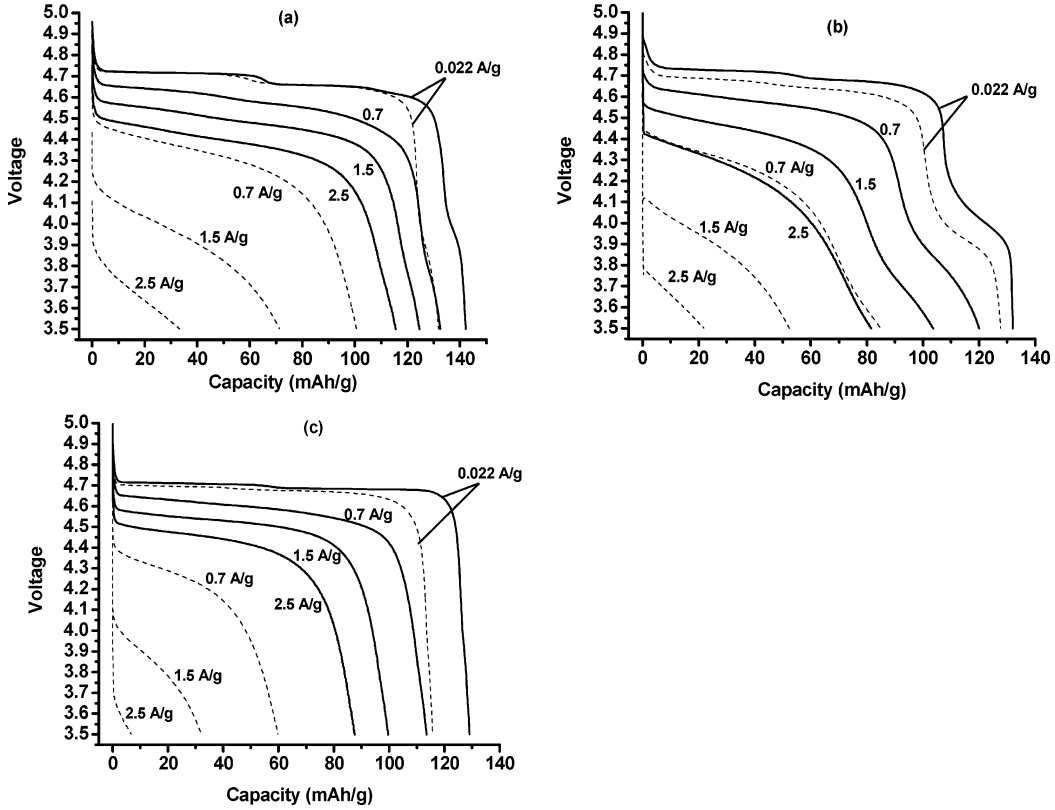

Figure 9. Galvanostatic discharge voltage curves of (a) Ni-0.49*, (b) Ni-0.40, and (c) Ni-0.50 samples with 4 wt % (dashed) and 13 wt % (solid) Super P. The numbers on the graph represent the discharge current densities in A/g.

than their 700 °C counterparts, possibly due to the increased content of Mn^{3+}, morphological changes, and/or oxygen loss, as evidenced by an increase in 4 V plateau (not shown), but also the performance gap between 730 and 700 °C samples widened at faster discharge rates. This result is further discussed later based on comparison of their morphological features studied with FESEM and HRTEM.

Representative galvanostatic discharge voltage curves of Ni-0.50, Ni-0.40, and Ni-0.49* are given in Figure 9 for different discharge rates and percentage of Super P (4 and 13 wt %). In all three samples, rate capability of the cathode material shows strong dependence on amount of Super P. All samples delivered much larger capacities with increasing use of conductive agent. A significant IR drop is observed with increasing current rates or decreasing percentage of conductive agent. The difference in IR drop and capacity retention grows in favor of disordered spinels (Ni-0.40 and Ni-0.49*) when wt % Super P $\leq$ 6.5 consistent with electronic vs ionic diffusion limitations.

The best performance was identified after annealing $LiMn_{1.51}Ni_{0.49}O_4$ directly at 730 °C for only 1 h without any pretreatment (denoted as Ni-0.49**). $LiMn_{1.51}Ni_{0.49}O_4$ was selected as the starting composition in order to maximize the capacity at 4.7 V. The initial discharge capacity at 22 mA/g was 133 mA·h/g. The 1st and 2nd cycle Coulombic efficiency of spinel were 82% and 95%, respectively. The spinel retained 95, 92, and 87% (=115.7 mA·h/g) of its capacity at 0.7 A/g (5.2 C), 1.5 A/g (11.2 C), and 2.5 A/g (18.8 C) discharge rates, respectively.

To evaluate faster charge rates, this material was cycled 245 times under galvanostatic conditions at 500 mA/g (3.8 C) and 2500 mA/g (~19 C) charge and discharge currents, respectively. As seen in Figure 10, the cell delivered a maximum discharge capacity of 113 mA·h/g (instead of 115.7 when charged at 22 mA/g). The spinel suffered a loss of only 2.5% after 245 cycles with a 99.85% Coulombic efficiency. After the 245th cycle, the discharge current was reduced to 22 mA/g. The capacity was 129.9 mA·h/g, resulting in an irreversible loss of only 2.3% (vs 133 mA·h/g). For an average discharge potential of 4.4 V and discharge current density at 2.5 A/g, the specific energy and power density of the spinel were calculated to be 490 W·h/kg and 11 kW/kg, respectively. The cell was able to sustain this power for 161 s.

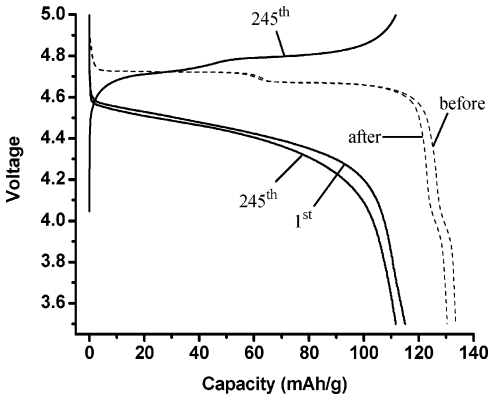

Figure 10. Galvanostatic charge/discharge curves of Ni-0.49**. The discharge current densities were 2500 mA/g (solid) and 22 mA/g (dashed). The before and after refer to "before the 1st" and "after the 245th" cycles, respectively. Charge current density was 500 mA/g.

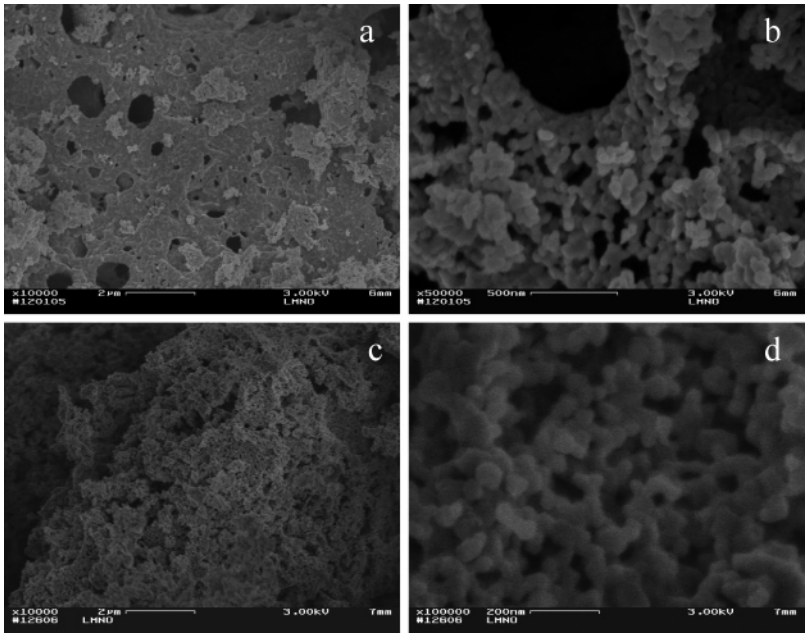

Figure 11. FESEM images of $LiMn_{1.6}Ni_{0.4}O_4$ (a,b) heat-treated at 700 °C for 15 h (Ni-0.40) and (c,d) postannealed at 730 °C for 2 h (Ni-0.40*) at different magnifications.

Morphological Considerations

Previously, we reported that the spinels we fabricated using the technique utilized in this paper contained a three-dimensional mesoporous network structure with nanosize particles. This morphology allows easy electrolyte penetration into pores and continuous interconnectivity of particles, yielding high power densities at fast discharges. Based on our experience and observations regarding the earlier and new powder synthesis paths, the rate capability has a strong dependence not only on electronic conductivity, as demonstrated here, but also morphological features of powder, especially at very high discharges rates (i.e., 2.5 A/g) used in this study.

In an effort to understand the basis of electrochemical improvement obtained with postannealing at 730 °C or direct heating to this temperature, we have characterized 700 and 730 °C spinels given in Table 1 by BET and FESEM. Figures 11a−d compare the morphological development of Ni-0.40 and Ni-40* spinels annealed at 700 °C for 15 h and postannealed at 730 °C for 2 h, respectively. It is seen that the above-mentioned mesoporous structure is not disturbed after heating to 730 °C. Also, as displayed better in images with higher magnification, the primary crystallite size and interparticle nanoporosity are approximately the same. The observation that the primary particle size and distribution is similar with or without postannealing is in agreement with BET surface area measurements reported in Table 1, namely, 6.17 and 5.42 m^2/g, respectively. Images do suggest the possibility of a thicker neck area between particles. Since resistance to electron flow is inversely proportional to the area of pathway taken by electrons, the enhancement in electrochemical performance may be attributed to improved electron transport.

When we annealed an ordered $P4_332$ Ni-0.49 sample to 730 °C to form a disordered $Fd3m$ Ni-0.49*, the drastically improved rate capability was attributed to the small degree of Mn^{3+} formed with the spinel. To further discount the formation of a surface layer formed during oxygen loss as

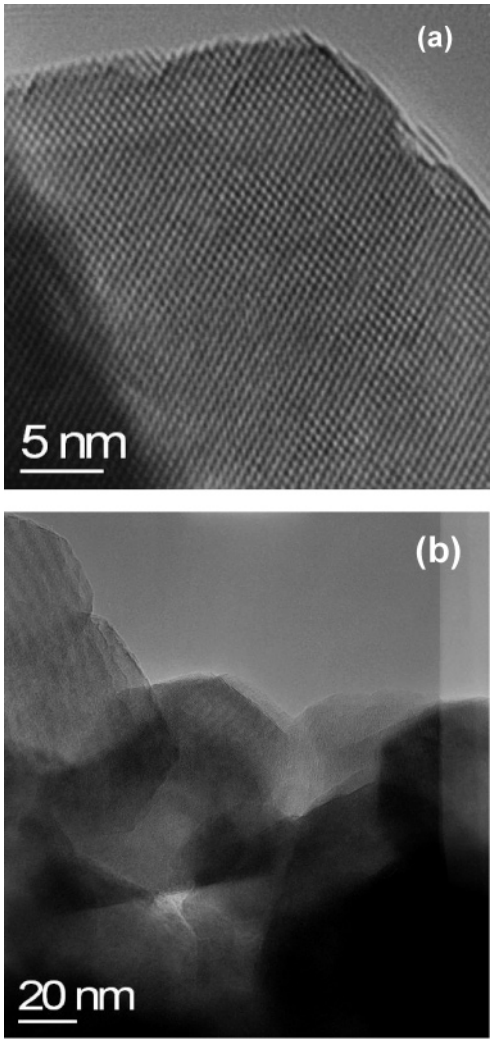

Figure 12. High-resolution TEM images of Ni-49* at various magnifications.

the basis for the high rate capability, HRTEM was performed on this sample. As shown in Figure 12, the crystallite has very clean lattice fringes extended to the surface of the spinel, discounting the presence of any surface phase.

Conclusion

We have demonstrated the correlation between the increase of the lattice constant of spinel $LiMn_{2-x}Ni_xO_4$ due to increased Mn^{3+} content and its electronic conductivity. The maximum difference in the electronic conductivity between cation ordered ($P4_332$) and disordered ($Fd3m$) spinel phases amounted to 2.5 orders of magnitude within the range of lattice constants studied. The electron hopping from increased content of Mn^{3+} to Mn^{4+} was explained as the basis of higher electronic conduction of disordered spinel than ordered spinel, which is absent of Mn^{3+}. By systematically altering the carbon black content in cathode electrode formulation and comparing spinels of various intrinsic electronic conductivities, we proved our earlier assertion that the ordered spinel is limited by its low electronic conductivity (10^{-7} S/cm at room temperature) when it comes to capacity retention at fast discharge rates.

We made use of this knowledge in designing a highly conductive spinel chemistry combined with a nanostructured network such that it delivers high capacities at fast discharge rates (approximately 90% utilization at 19 C). The resulting material not only showed excellence in terms rate capability but also had very good capacity maintenance at accelerated electrochemical cycling at 24 °C. We expect elevated temperature cycling to be more challenging due to high-voltage interactions with the electrolyte. It is clear, however, that the final optimization of the material will depend on a coordinated design of the bulk nanostructure relative to a delicate balance between intrinsic ionic and electronic conductivities offset by macro electrode composition crutches such as carbon black.

Acknowledgment. The authors would like to thank the U.S. Government for financial support of this research. The authors would also like to thank J. Gural for fabrication of items crucial to measurements made throughout this work.

CM060729S